Check for updates

ADVANCED FUNCTIONAL MATERIALS
www.afm-journal.de

Perovskite Nanocrystals Initiate One-Step Oxygen Tolerant PET-RAFT Polymerization of Highly Loaded, Efficient Plastic Nanocomposites

Valentina Bellotti, Francesco Carulli, Sara Mecca, Matteo L. Zaffalon, Andrea Erroi, Federico Catalano, Matteo Boventi, Ivan Infante, Francesca Rossi, Luca Beverina, Sergio Brovelli, and Roberto Simonutti**

Lead halide perovskite nanocrystals (LHP-NCs) incorporated within polymer matrices have emerged as promising materials for various photonic applications. However, challenges persist in achieving high-quality nanocomposites due to low monomer conversion yields, restricted LHP-NCs loadings, and difficulty in maintaining NCs integrity post-polymerization. A novel protocol for synthesizing LHP-NCs/poly(methyl methacrylate) nanocomposites in a single step via the NC-initiated photoinduced electron transfer-reversible addition-fragmentation chain transfer (PET-RAFT) method is presented. Polymerization initiation mediated by NCs surfaces under blue light enables the fabrication of homogeneous nanocomposites with NCs loadings up to 7% w/w and ≈90% monomer conversion even in the presence of oxygen. This process preserves the optical quality of the NCs and passivates NCs surface defects, resulting in nanocomposites exhibiting near unity luminescence efficiencies. The potential of this approach for producing highly loaded nanocomposites for radiation detection is validated by radioluminescence measurements showing light yield values of 6000 ph MeV^{-1} and fast scintillation dynamics with effective lifetime of 490 ps, showing promise for time-of-flight radiometry.

1. Introduction

Lead halide perovskite nanocrystals (LHP-NCs), represented by the formula $APbX_3$ (where A = $CH_3NH_3^+$, $CH(NH_2)_2^+$, Cs and X = Cl, Br, I), have garnered significant attention in various technological domains over the past decade.[1] The interest in these materials stems from their notable characteristics, including bright and narrow-band photoluminescence (PL) with tunable emission across the visible spectrum,[2] excellent PL quantum yield (PLQY),[1b,3] high absorption coefficient,[4] defect tolerance,[5] long exciton diffusion length,[6] and low exciton binding energies.[7] Particularly, LHP-NCs have emerged as versatile candidates for efficient light emission in applications such as artificial lighting,[2a,8] displays,[9] luminescent solar concentrators,[10] and scintillator detectors for radiometric purposes.[11] However, despite their promising characteristics, LHP-NCs are plagued by long-term instability, sensitivity to moisture, oxygen, and thermal factors, as well as limited processability, which hinder their effectiveness for potential applications.[12] To address these challenges, acrylic and methacrylic polymers, such as poly(methyl methacrylate) (PMMA) or polystyrene (PS), have been employed to encapsulate LHP-NCs.[13] This encapsulation serves the dual purpose of producing manageable solid objects

V. Bellotti, F. Carulli, S. Mecca, M. L. Zaffalon, A. Erroi, M. Boventi, L. Beverina, S. Brovelli, R. Simonutti
Dipartimento di Scienza dei Materiali
Università degli Studi di Milano-Bicocca
via R. Cozzi 55, Milano 20125, Italy
E-mail: sergio.brovelli@unimib.it; roberto.simonutti@unimib.it

F. Catalano
Electron Microscopy Facility
Istituto Italiano di Tecnología
via Morego 30, Genova IT-16163, Italy

I. Infante
BCMaterials
Basque Center for Materials
Applications
and Nanostructures
UPV/EHU Science Park
Leioa 48940, Spain

F. Rossi
IMEM-CNR Institute
Parco Area delle Scienze 37/A, Parma 43124, Italy

The ORCID identification number(s) for the author(s) of this article can be found under https://doi.org/10.1002/adfm.202411319

© 2024 The Author(s). Advanced Functional Materials published by Wiley-VCH GmbH. This is an open access article under the terms of the Creative Commons Attribution License, which permits use, distribution and reproduction in any medium, provided the original work is properly cited.

DOI: 10.1002/adfm.202411319

for integration into device schemes and enhancing their stability, processability, and optical properties by passivating charge traps. While the use of PS for the mass polymerization of LHP-NCs nanocomposites is hindered by the high polymerization temperatures required, which can lead to particle degradation,[14] PMMA offers an advantage as it can be optically mass-polymerized at lower temperatures that are tolerated by the LHP-NCs.[11c,15] PMMA is a well-established commercial polymer with excellent characteristics for fabricating plastic nanocomposites.[16] Its high glass transition temperature provides mechanical stability, and it offers simple manufacturing processes, and good optical properties. Current methods for fabricating LHP-NCs/polymer composites primarily rely on three approaches: i) physically embedding LHP-NCs into a polymer matrix using the solvent evaporation method,[17] ii) directly synthesizing LHP-NCs within a polymer solution via thermal annealing,[18] and iii) conducting in situ mass polymerization of the polymer matrix in the presence of the NCs.[15]

However, each of these techniques comes with its own set of drawbacks. The solvent evaporation method, for instance, is not suitable for large-scale production, involves the use of toxic solvents, and tends to yield inhomogeneous composites with limited size control.[19] Direct synthesis of LHP into polymer solution often results in uncontrolled NCs size and aggregation, thereby impacting the optical quality of the resulting composite. In situ polymerization, while appealing for bulk nanocomposite production, typically relies on radical photoinitiators, such as 2,2-dimethoxy-2-phenylacetophenone, activated under UV illumination (typically at 365 nm). This UV light reliance limits the maximum NCs loading due to competitive light absorption. Furthermore, these photoinitiators may potentially damage the photophysical properties of the NCs, leading to lower PLQY.[20] Both the Lalevée and Tan groups have demonstrated that the use of UV photoinitiators can be circumvented by leveraging the LHP-NCs themselves as initiators for free radical polymerization (FRP).[21] While this approach resulted in improved optical properties of the nanocomposites and good dispersity of the NCs, it led to lower polymerization conversion and NC loading. The limitations of LHP-NCs-initiated FRP in terms of monomer conversion and particle loading are interconnected and stem from the uncontrolled nature of the polymerization technique, a high initiator concentration (i.e., the NCs loading) negatively affects polymer chain termination.[22] On the other hand, the selection of a more controlled radical polymerization technique, such as the family of reversible deactivation radical polymerization (RDRP) allows for a constant radical concentration during polymerization, independent of the initiator amount, potentially enabling higher LHP-NCs loading.[23] Of the RDRP strategies, reversible addition-fragmentation chain-transfer (RAFT) polymerization, together with the more recent photocatalyzed PET (photoinduced electron transfer)-RAFT polymerization, are arguably two of the more versatile strategies.[24] The initial work by Egap et al.[25] and subsequent research by Gao et al.[26] have demonstrated the remarkable capability of $CsPbX_3$ NCs to act as photoinitiators in PET-RAFT polymerization.[27] This discovery offers significant advantages for the preparation of highly loaded LHP-NCs/polymer nanocomposites: i) In RDRP, the amount of initiator does not affect the polymerization yield, enabling the one-step synthesis of bulk composites with high NCs content as photocatalysts (PCs). ii) The activation of the chain transfer agent (CTA) by photoexcited NCs occurs at the catalyst interface.[24a,28] iii) Lewis bases, particularly sulfur-based compounds like thiocarbonylthio-containing CTAs, exhibit strong electron-donating properties, making them ideal candidates for coordination with electron-deficient Pb atoms.[29] This facilitates the PET process, prevents NCs agglomeration in the polymer matrix, and helps passivate surface traps associated with undercoordinated Pb cations, ultimately improving the optical properties of the nanocomposite.

Despite significant progress in this field, low polymerization yields and satisfactory LHP-NCs loadings remain common challenges for most reported in situ polymerization techniques. Addressing these challenges, we present an efficient protocol for preparing $CsPbBr_3$ NCs-PMMA nanocomposites in a one-pot, one-step process through LHP-NCs-initiated PET-RAFT polymerization. The composites were synthesized at room temperature, in the presence of oxygen, and without generating toxic waste containing heavy metal ions. We achieved a remarkable monomer conversion of methyl methacrylate (MMA) close to 90%, along with high LHP-NCs loadings (up to 7%). The embedding process, monitored in situ during the polymerization reaction and investigated theoretically via density functional theory calculations, induced a positive evolution of the NCs in the polymer matrix, enhancing their emission efficiency by suppressing shallow surface traps. Consequently, the $CsPbBr_3$ NCs served a dual role as a blue light photocatalyst for the controlled polymerization of highly loaded PMMA nanocomposites and efficient emitters for photonic applications, directly encapsulated in a solid bulk polymer matrix.

2. Results and Discussion

2.1. Kinetics and Performance of $CsPbBr_3$ NCs Initiated PET-RAFT

The $CsPbBr_3$ NCs were synthesized according to our recently introduced turboemulsified room-temperature process,[30] which allows the large-scale synthesis of NCs (up to 8 g per batch) and the recycling of the waste generated during NCs production, which is very attractive for the production of high-load nanocomposites in large quantities. According to what is typically observed for room temperature reprecipitation methods,[31] the as-synthesized crude product comprised NCs with mixed dimensionality (see high resolution scanning tunnelling micrograph in Figure S1, Supporting Information, and corresponding elemental composition in Figure S2, Supporting Information) with a dominant population of brick-like NCs with an average size of 13 ± 3 nm and thickness of 5 ± 1 nm (**Figures** 1a and S1, Supporting Information), as further confirmed by the absorption profile in Figure 1b showing a low energy shoulder ascribed to larger structures in the ensemble. The corresponding PL spectrum in toluene peaked at 514 nm with full width at half maximumum of FWHM = 23 nm and PLQY = 64%.

The polymerization of MMA was carried out with 2-cyano-2-propylbenzodithioate (CPDB) as CTA (M/CTA = 800) under semi-bulk conditions (Figure 1c). With a very low amount of photocatalytic NCs (0.05 wt% with respect to the monomer), a conversion of 87.1% was obtained after 24 h under 460 nm

© 2024 The Author(s). Advanced Functional Materials published by Wiley-VCH GmbH

16163028, 0, Downloaded from https://onlinelibrary.wiley.com/doi/10.1002/adfm.202411319 by Universita Milano Bicocca, Wiley Online Library on [07/10/2024]. See the Terms and Conditions (https://onlinelibrary.wiley.com/terms-and-conditions) on Wiley Online Library for rules of use; OA articles are governed by the applicable Creative Commons License

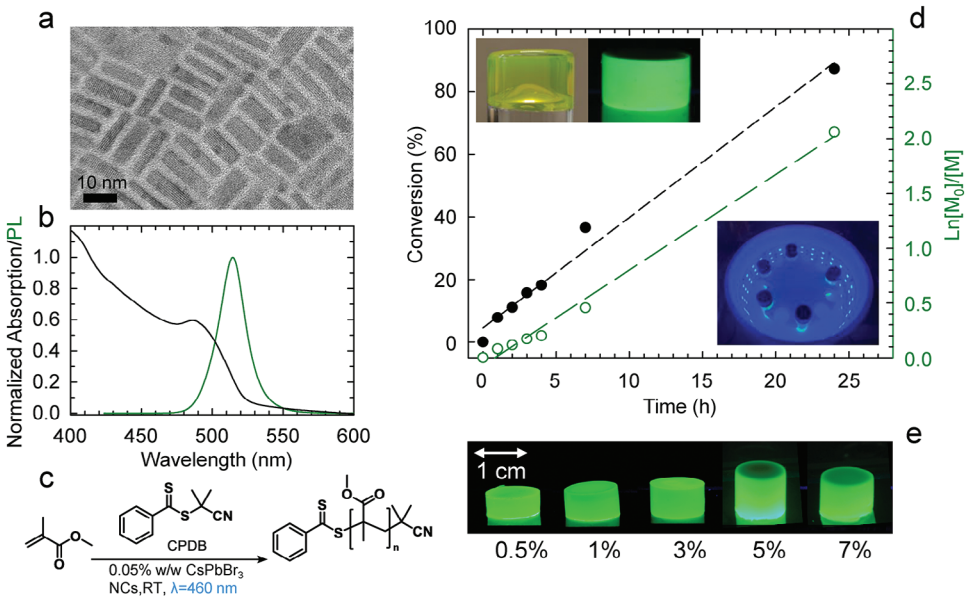

Figure 1. a) Transmission electron microscopy image of $CsPbBr_3$ NCs with average size of 13 ± 3 nm and thickness of 5 ± 1 nm. b) Optical absorption and PL spectrum of $CsPbBr_3$ NCs in toluene. c) Reaction scheme of PET-RAFT polymerization of MMA under blue irradiation with CPDB as chain transfer agent. d) Kinetic of the polymerization (0.05 wt% of PC) showing a linear conversion of the monomer over time with a pseudo first-order kinetic. Inset: Photograph of the reaction setup and the final solid sample after 24 h under irradiation. e) Photograph of bulk PMMA samples embedding increasing NCs content up to 7 wt% before cutting to the same size (1.4 cm diameter and 0.5 cm height).

blue light irradiation and the consequent one-pot formation of $CsPbBr_3$-PMMA bulk without any purification step (**Table 1**, entry 4). The progress of the polymerization over time was monitored by ^{1}H NMR of the reaction crude. The linear increase of the conversion with time identifies a pseudo first order kinetic (Figure 1d), confirming that the polymerization follows the RDRP behavior, as expected for the PET-RAFT mechanism (Figure S3, Supporting Information). As the polymerization progressed, the viscosity increased as expected for a bulk polymerization. In fact, the 90% conversion is close to the maximum achievable value due to the high stiffness of the sample, which no longer allows the monomer to diffuse.[32] Consistent with previous reports,[21b,33] negligible conversion was obtained in the absence of light, whereas, when the polymerization was performed in the presence of CTA and without the $CsPbBr_3$ NCs, PMMA was obtained with drastically lower conversion. Finally, in the presence of $CsPbBr_3$ NCs but without the CTA, the polymerization produced very high molecular weight but in an uncontrolled fashion, as demonstrated by the high polydispersity of the molecular weights ($Đ = 2.3$) (Table 1, entries 1–3).

Table 1. PET-RAFT polymerization of methyl methacrylate (MMA) using $CsPbBr_3$ in toluene as photocatalyst and CPDB as chain transfer agent. Reactions were conducted under 460 nm blue light, at room temperature for 24 h.

Entry	[M]/[CPDB]	PC loading [wt%]	α[a)] [%]	$M_{n,GPC}$[b)]	$Đ$[b)]
1[c)]	800	0.05	–	–	–
2	800	–	18.2	21 800	1.12
3	–	0.05	37.5	330 000	2.3
4	800	0.05	87.1	81 000	1.3
5	400	0.05	87.0	39 000	1.24
6	200	0.05	89.2	24 900	1.16
7	100	0.05	88.8	12 800	1.12
8	800	0.5	87.6	93 000	1.28
9	800	1	88.7	101 300	1.26
10	800	3	87.9	97 200	1.24
11	800	5	85.0	112 400	1.35
12	800	7	78.8	92 000	1.27

[a)] Monomer conversion (α) calculated with NMR analysis; [b)] Molecular weight and dispersity were obtained by gel permeation chromatography (GPC) measures. Entries from 8 to 12 have been polymerized in oxygenated environment with the addition of limonene as oxygen quencher; [c)] Entry 1 experiment was performed without light irradiation. [M]/[CPDB] is the ratio between the concentration of monomer and charge transfer agent.

The polymerization was further repeated by decreasing the monomer-to-CTA molar ratio (from 800 to 100), maintaining the $CsPbBr_3$ NCs concentration constant (Table 1, entries 5–7). In all cases, a yield close to 90% was obtained with a consequent increase of the molecular weight with decreasing CTA molar content. Low dispersity values ($1.12 < Đ < 1.3$) were maintained for all the polymerizations indicating that the chains grew in a control fashion, with a degree of polymerization close to the theoretical one, even at high monomer-to-CTA ratio.

Next, we demonstrated the effectiveness of PET-RAFT polymerization in producing highly loaded nanocomposites by increasing the NCs concentration up to 7 wt% with respect to the monomer, as shown in Table 1, entries 8–12, and confirmed by thermogravimetric analysis (**Figure 2a**). TEM analysis of different sections of the material at different depths confirmed the dispersibility of the embedded NCs in the polymer matrix (Figure 2b), supporting the interaction of the CTA with the

© 2024 The Author(s). Advanced Functional Materials published by Wiley-VCH GmbH

16163028, 0, Downloaded from https://onlinelibrary.wiley.com/doi/10.1002/adfm.202411319 by Universita Milano Bicocca, Wiley Online Library on [07/10/2024]. See the Terms and Conditions (https://onlinelibrary.wiley.com/terms-and-conditions) on Wiley Online Library for rules of use; OA articles are governed by the applicable Creative Commons License

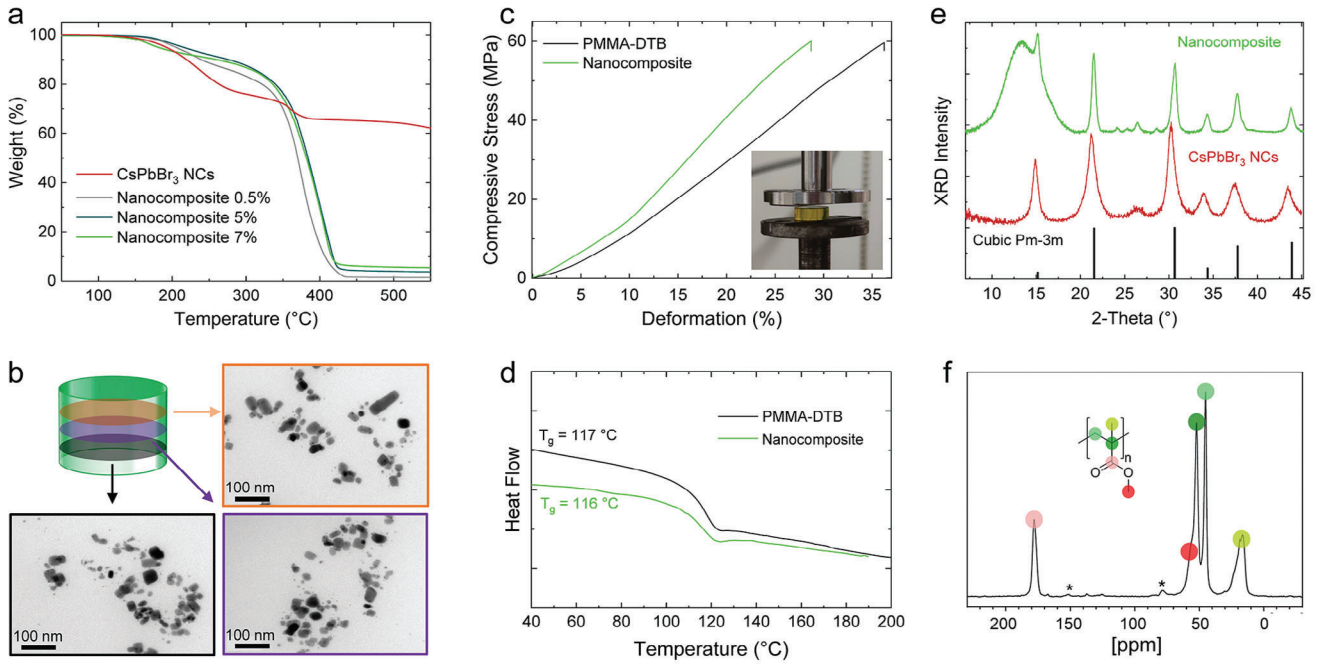

Figure 2. a) Thermogravimetric analysis (TGA) of the nanocomposites with 0.5, 5, and 7 wt% loadings, compared to the native NCs (red line). The weight loss in the native NCs is attributed to the ligand surface coverage. b) TEM micrographs of three different 70 nm thin nanocomposite sections obtained from entry 11, Table 1 (0.5 cm thick). c) Compressive test and d) Differential scanning calorimetry (DSC) measurements of the nanocomposite material (green line) compared to PMMA synthetized by RAFT polymerization with the same chain length and CTA (black line). e) Powder X-ray diffraction patterns of the nanocomposites with 7 wt% of embedded NCs (top, green line), the native NCs (middle, red line), and the calculated power X-ray diffraction (PXRD) pattern for cubic $CsPbBr_3$. The broad peak at 15° is due to the PMMA matrix. f) ^{13}C cross polarization magic angle spinning (CPMAS) spectrum of the nanocomposite with 7 wt% loading acquired at 10 kHz speed, showing no peaks in the alkene region (120–150 ppm). * refers to spinning sidebands.

surface of the NCs as polymerization proceeds. The mechanical stability of PMMA was not affected by the presence of increased NCs loading, as demonstrated by the compression test (Figure 2c), consistent with the high glass transition temperature (116 °C, Figure 2d) characteristic of PMMA. Finally, the crystalline structure of the NCs was preserved during synthesis. However, it is plausible that part of the NCs oriented toward the orthorhombic phase (peaks 10°–20°) due to the distortion caused by the new synthetized rigid polymer matrix (Figure 2e). Finally, to further improve the processability and scalability of our methodology, the polymerizations were carried out in the presence of oxygen by adding limonene as an oxygen quencher, further simplifying the synthetic procedure. The unreacted monomer was simply removed by evaporation at room temperature and atmospheric pressure, resulting in the complete absence of monomer as demonstrated by solid state NMR (Figure 2f).

2.2. Mechanistic Evaluation of $CsPbBr_3$ Initiated PET-RAFT

In order to investigate the mechanism of the NCs-activated polymerization reaction and clarify the evolution of the optical properties of the as-synthesized NCs inside the polymer host, which represents a further technological advantage of the NCs-initiated PET-RAFT process, we monitored the photoluminescence spectrum and time kinetics during the various stages of the process. As schematically depicted in **Figure** 3a, the addition of the CTA into the MMA-NCs mixture prompts the *initiation* stage where the surface interaction of the CTA moieties activates the electron transfer process from photoexcited NCs. This is followed by the *propagation* stage characterized by progressive chain growth until the complete consumption of monomers that determines the end of reaction. The final nanocomposites contain NCs surrounded by the polymer chains. The effects of these interactions on the optical properties of the NCs are shown in Figure 3b,c where we report the PL spectra and decay traces versus reaction time and in Figure S4 in the Supporting Information comparing the optical absorption and PL spectra of the NCs in solution and the final composite. The spectrally integrated intensity and lifetime $<\tau>$ (expressed as the time after which the PL intensity decreased by a factor *e*), are shown in Figure 3d,e. The initiation phase was associated with a steep quenching of the PL intensity and $<\tau>$ due to electron transfer from the NCs to the CTA. This was further confirmed by the acceleration of the emission dynamics with increasing CTA concentration in toluene, which followed the characteristic exponential trend expected for charge transfer processes (Figure S5, Supporting Information). As the reaction progressed to the propagation stage, the PL gradually intensified and slowed down, finally reaching a plateau corresponding to near unity PLQY values than the initial monomer solution (PLQY = 84%). Interestingly, this behavior was accompanied by a nonmonotonic evolution of the emission profile (Figure S6, Supporting Information), quantified in terms of the FWHM with reaction time (Figure 3d). Specifically, in the initiation phase, the rise of a high

© 2024 The Author(s). Advanced Functional Materials published by Wiley-VCH GmbH

16163028, 0, Downloaded from https://onlinelibrary.wiley.com/doi/10.1002/adfm.202411319 by Universita Milano Bicocca, Wiley Online Library on [07/10/2024]. See the Terms and Conditions (https://onlinelibrary.wiley.com/terms-and-conditions) on Wiley Online Library for rules of use; OA articles are governed by the applicable Creative Commons License

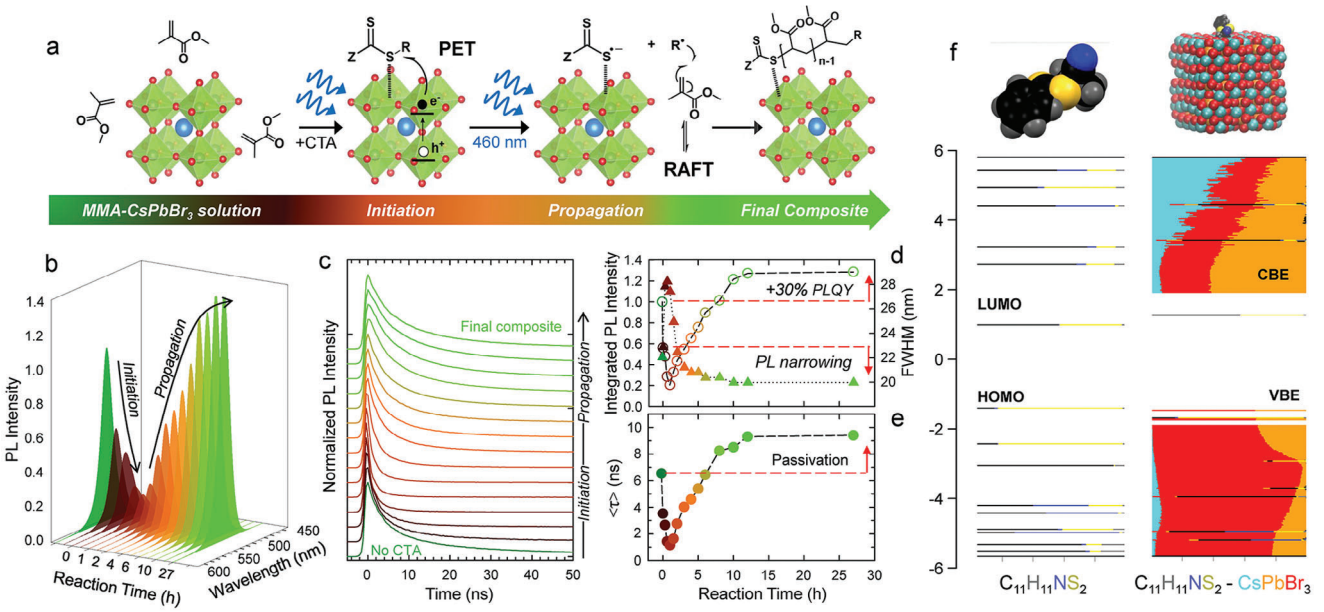

Figure 3. a) Reaction scheme of the $CsPbBr_3$-initiated PET-RAFT polymerization of PMMA. b) PL spectra and corresponding c) decay curves of the nanocomposite during the polymerization reaction at room temperature under blue light irradiation (0.05% NCs loading and [M]/[CTA] = 800). d) Integrated PL intensity and FWHM values extracted from "b". e) Effective PL lifetimes extracted from "c" versus reaction time. f) Energy levels of the CTA and g) density of states of LHP-CTA. Each horizontal line corresponds to a molecular orbital (MO). The length of the colored line segments indicates the contribution of each element to an MO. HOMO, LUMO, conduction band (CBE), and valence band (VBE) levels of the nanocrystal are highlighted.

energy shoulder of the PL peak led to a spectral broadening from 23 to 28.5 nm, followed by a gradual narrowing of the emission linewidth during the propagation phase, ultimately leading to narrower PL profiles (FWHM = 20 nm) than the as-synthesized particles. This, together with the PL intensity trend, suggests NCs ripening triggered by the interaction with the CTA moieties, increasing the population of smaller particles in the ensemble, followed by a uniformation of the NCs towards cuboidal shapes and suppression of phononic disorder in the final composite accompanied by surface curing by the polymer chains, in agreement with recent observation.[25] These aspects are expanded in Figure S7 in the Supporting Information including the analysis of PL kinetics using a double-exponential decay model which traces the interplay between the band edge (BE) exciton and shallow defect states, as well as their interaction with the polymerization environment throughout the process. In order to better understand the mechanisms of excitation transfer and binding of the CTA to the surface, we have modeled a $CsPbBr_3$ nanocrystal using density functional theory (DFT) and evaluated the position of the energy levels (density of states) of CTA and of the LHP-CTA system, as shown in Figure 3f,g. The CTA molecule appears to be loosely bound to the surface of the nanocrystal, as its binding energy is about 5 kcal mol^{-1}. This is reflected in the energy levels that change very little when CTA is in proximity of the surface. Irrespective of this, the energy of the highest occupied molecular orbital and the lowest unoccupiued molecular orbital (HOMO-LUMO) allows charge transfer from the photoexcited nanocrystal to the CTA, promoting homolytic cleavage of the C-S CTA's bond into ZSS and R fragments, and initiating polymerization. We also evaluated with DFT two possible final configurations after the polymer ZSS-$(MMA)_n$-R is formed near the NCs surface, where ZSS and R are the two parts of CTA. The first is with R-$(MMA)_n$ and *Z* radicals directly bound to the NCs, i.e., the nanocrystal directly closes the polymer chain on one side and is partially passivated by the sulfur part of the CTA on two different binding sites and another one in which ZSS-$(MMA)_n$-R sits in proximity of the surface. We found the latter more stable of about >20 kcal mol^{-1}, indicating a strong preference for the latter. Besides this, to explain the increase in quantum yield as a result of polymerization, a more detailed study is required, as it is necessary to investigate how the polymer chains interact with the surface of the nanocrystal with the complete ligand shell attached to it.

2.3. PET-RAFT-Based Perovskite Nanocomposites for Scintillation

Finally, with a view to testing the potential of PET-RAFT polymerization to produce high performance materials for a highly topical application that specifically requires high loads of perovskite NCs in massive samples,[15,19,34] namely the detection of ionizing radiation, we investigated the scintillation properties of our nanocomposite materials. Radiation detection typically relies on inorganic crystals[35] or plastic scintillators,[36] which suffer from high cost or weak interaction with high energy radiation due to insufficient average atomic number (*Z*) composition, which determines the interaction probability with ionizing radiation ($P \sim Z^n$ with $n = 1$–5 depending on the type of interaction).[37] Therefore, the ability of NCs-initiated PET-RAFT photopolymerization to realize highly loaded nanocomposites is highly valuable to overcome the shortcomings of

© 2024 The Author(s). Advanced Functional Materials published by Wiley-VCH GmbH

16163028, 0, Downloaded from https://onlinelibrary.wiley.com/doi/10.1002/adfm.202411319 by Universita Milano Bicocca, Wiley Online Library on [07/10/2024]. See the Terms and Conditions (https://onlinelibrary.wiley.com/terms-and-conditions) on Wiley Online Library for rules of use; OA articles are governed by the applicable Creative Commons License

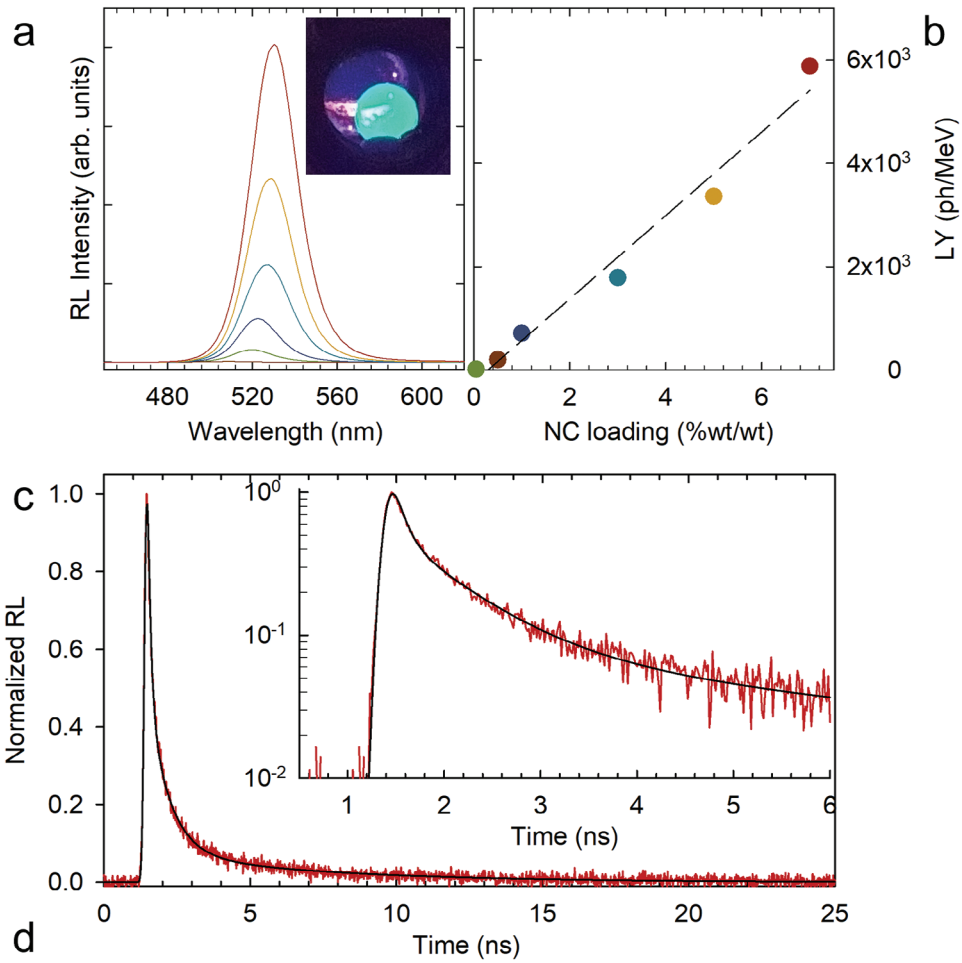

d

τ_1	w_1 (%)	τ_2	w_2 (%)	τ_3	w_3 (%)	τ_{eff}	CTR (estimated)
100 ps	15	703 ps	36	5870 ps	49	490 ps	11.6 ps

Figure 4. a) Radioluminescence (RL) spectra of $CsPbBr_3$ NCs-based PMMA nanocomposites with increasing particle loading (Inset: picture of a representative nanocomposite under X-ray excitation) and b) respective LY values measured through comparison of the integrated RL intensity of an EJ276D scintillator). c) RL decay curve and respective fitting curve. The same color scheme applies throughout the figure. d) Fit parameters (decay time and relative integrated weight, w_i) used to analyze the time-resolved RL intensity decay. The RL dynamics were analyzed in a least squares sense using a triple exponential function convolved with the instrument response function. The effective decay time (τ_{eff}) was calculated using the normalized ratio of all the components according to $\tau_{eff}^{-1} = \sum_{i=1}^{3} R_i/\tau_i$, $R_i = w_i / (w_1 + w_2 + w_3)$. The coincidence time resolution (CTR) has been estimated using the formula indicated in the main text, where the 10–90% rise time (τ_{rise}) was set to 80 ps, and the estimated number of photons emitted for a 511 keV excitation was set to $N = 3240$.

existing motifs through a nanocomposite scintillator approach.[19] With this in mind, we performed *cw* and time-resolved radioluminescence experiments using soft X-rays as excitation source. **Figure** 4a shows the RL spectra of PMMA-NCs nanocomposites with increasing NCs mass concentration. The corresponding light yield (LY) values, obtained by comparing the RL intensity of the samples with a calibrated plastic scintillator (EJ276D) of the same dimensions (thickness 0.5 cm) and excitation/detection conditions, are shown in Figure 4b. The RL spectra are very similar to the corresponding PL and intensify linearly with the NCs loading, with a slight concomitant redshift due to partial reabsorption of the scintillation light—note that the X-rays (average energy 7 keV) are completely absorbed by the whole sample thickness (ca. 0.7 cm) and therefore the scintillation light produced in the depth of the nanocomposite body is affected by progressively stronger reabsorption with increasing NCs loading. Nevertheless, the light yield (defined as the number of emitted photons per unit energy deposited in the material) reaches LY = 6000 ph MeV^{-1}, which is close to a commercial plastic scintillator (LY_{EJ276D} = 8600 ph MeV^{-1})[38] without any specific compositional optimization such as the addition of secondary emitters in engineered cascade energy transfer schemes. The absence of spurious intragap emissions in the RL spectrum confirms suppression of shallow and deep traps in agreement with the near unity PL efficiency.[39]

© 2024 The Author(s). Advanced Functional Materials published by Wiley-VCH GmbH

16163028, 0, Downloaded from https://onlinelibrary.wiley.com/doi/10.1002/adfm.202411319 by Universita Milano Bicocca, Wiley Online Library on [07/10/2024]. See the Terms and Conditions (https://onlinelibrary.wiley.com/terms-and-conditions) on Wiley Online Library for rules of use; OA articles are governed by the applicable Creative Commons License

We further interrogated the timing performance of our nanocomposites using pulsed X-rays. The RL decay curve of a nanocomposite with 7% NCs loading is shown in Figure 4c. Consistent with previous reports on LHP-based scintillators,[17a,19,30,40] the kinetics are ultrafast with sub-nanosecond components ascribed to the recombination of charged- and biexciton species created upon interaction with ionizing radiation followed by the ns-long luminescence due to single exciton decay. To extract an effective lifetime τ_{EFF} that is typically used as a figure of merit of the scintillation timing performance, we fitted the experimental data with a triple exponential function representing the above-mentioned decay contributions[40] convoluted with the instrument response function of our detection chain. The fitting parameters are reported in Figure 4d. The weighted harmonic average of the decay components yields $\tau_{EFF} = 490$ ps that combined with the estimated number of photons emitted for a 511 keV excitation (corresponding to the gamma energy employed in time-of-flight positron emission tomography) set to $N = 3240$ (consistent with the measured LY = 6000 ph MeV^{-1}) produces a potential coincidence time resolution,[41] CTR $= 3.33\sqrt{(\tau_{RISE} \times \tau_{EFF})/N} = 11.6$ ps, which is very promising for fast timing scintillation applications.[19,42]

3. Conclusions

In conclusion, we have presented the use of PET-RAFT technology as an efficient polymerization technique for the synthesis of $CsPbBr_3$ NCs/PMMA nanocomposites in a one-pot, one-step fashion. This method allowed a high reaction yield (around 90%) of MMA combined with a positive evolution of the NCs into a uniform ensemble, improving the optical properties of the final material. The controlled nature of the PET-RAFT polymerization is an additional advantage for the synthesis of highly loaded composites, maintaining a high polymerization yield and compatibilization of the NCs with the polymer matrix, which is extremely valuable for technologies requiring high loading of particles incompatible with high temperature processes such as LHP-NCs. The RDRP nature of the polymerization, combined with the oxygen tolerance of the technique and the multigram scale protocol for the synthesis of LHP NCs, opens the possibility of large-scale production of nanocomposites for light management technologies such as the detection of ionizing radiation, which is demonstrated with very promising scintillation performance.

Supporting Information

Supporting Information is available from the Wiley Online Library or from the author.

Acknowledgements

This work was funded by Horizon Europe EIC Pathfinder program through project 101098649 – UNICORN, by the PRIN program of the Italian Ministry of University and Research (IRONSIDE project), by the European Union—NextGenerationEU through the Italian Ministry of University and Research under PNRR—M4C2-I1.3 Project PE_00000019 "HEAL ITALIA", by European Union's Horizon 2020 Research and Innovation programme under Grant Agreement No 101004761 (AIDAINNOVA). This research was funded and supervised by the Italian Space Agency (Agenzia Spaziale Italiana, ASI) in the framework of the Research Day "Giornate della Ricerca Spaziale" initiative through the contract ASI N. 2023-4-U.0.

Open access publishing facilitated by Universita degli Studi di Milano-Bicocca, as part of the Wiley - CRUI-CARE agreement.

Conflict of Interest

The authors declare no conflict of interest.

Data Availability Statement

The data that support the findings of this study are available from the corresponding author upon reasonable request.

Keywords

lead halide perovskite nanocrystals, nanocomposites, PET-RAFT polymerization, photonics, scintillators

Received: June 27, 2024
Revised: August 12, 2024
Published online:

[1] a) A. Dey, J. Ye, A. De, E. Debroye, S. K. Ha, E. Bladt, A. S. Kshirsagar, Z. Wang, J. Yin, Y. Wang, L. N. Quan, F. Yan, M. Gao, X. Li, J. Shamsi, T. Debnath, M. Cao, M. A. Scheel, S. Kumar, J. A. Steele, M. Gerhard, L. Chouhan, K. Xu, X.-g. Wu, Y. Li, Y. Zhang, A. Dutta, C. Han, I. Vincon, A. L. Rogach, et al., *ACS Nano* **2021**, *15*, 10775; b) J. Shamsi, A. S. Urban, M. Imran, L. De Trizio, L. Manna, *Chem. Rev.* **2019**, *119*, 3296; c) P. Ramasamy, D.-H. Lim, B. Kim, S.-H. Lee, M.-S. Lee, J.-S. Lee, *Chem. Commun.* **2016**, *52*, 2067; d) A. P. Schlaus, M. S. Spencer, X. Y. Zhu, *Acc. Chem. Res.* **2019**, *52*, 2950; e) A. Ren, H. Wang, W. Zhang, J. Wu, Z. Wang, R. V. Penty, I. H. White, *Nat. Electron.* **2021**, *4*, 559; f) Y. Zhang, J. Liu, Z. Wang, Y. Xue, Q. Ou, L. Polavarapu, J. Zheng, X. Qi, Q. Bao, *Chem. Commun.* **2016**, *52*, 13637; g) R. J. Sutton, G. E. Eperon, L. Miranda, E. S. Parrott, B. A. Kamino, J. B. Patel, M. T. Hörantner, M. B. Johnston, A. A. Haghighirad, D. T. Moore, H. J. Snaith, *Adv. Energy Mater.* **2016**, *6*, 1502458.

[2] a) J. Song, J. Li, X. Li, L. Xu, Y. Dong, H. Zeng, *Adv. Mater.* **2015**, *27*, 7162; b) I. Levchuk, A. Osvet, X. Tang, M. Brandl, J. D. Perea, F. Hoegl, G. J. Matt, R. Hock, M. Batentschuk, C. J. Brabec, *Nano Lett.* **2017**, *17*, 2765; c) Q. A. Akkerman, V. D'Innocenzo, S. Accornero, A. Scarpellini, A. Petrozza, M. Prato, L. Manna, *J. Am. Chem. Soc.* **2015**, *137*, 10276.

[3] a) Q. A. Akkerman, G. Rainò, M. V. Kovalenko, L. Manna, *Nat. Mater.* **2018**, *17*, 394; b) F. Liu, Y. Zhang, C. Ding, S. Kobayashi, T. Izuishi, N. Nakazawa, T. Toyoda, T. Ohta, S. Hayase, T. Minemoto, K. Yoshino, S. Dai, Q. Shen, *ACS Nano* **2017**, *11*, 10373; c) A. F. Gualdrón-Reyes, S. Masi, I. Mora-Seró, *Trends Chem.* **2021**, *3*, 499.

[4] a) J. De Roo, M. Ibáñez, P. Geiregat, G. Nedelcu, W. Walravens, J. Maes, J. C. Martins, I. Van Driessche, M. V. Kovalenko, Z. Hens, *ACS Nano* **2016**, *10*, 2071; b) V. K. Ravi, G. B. Markad, A. Nag, *ACS Energy Lett.* **2016**, *1*, 665.

[5] a) B. A. Koscher, J. K. Swabeck, N. D. Bronstein, A. P. Alivisatos, *J. Am. Chem. Soc.* **2017**, *139*, 6566; b) S. Seth, T. Ahmed, A. De, A. Samanta, *ACS Energy Lett.* **2019**, *4*, 1610; c) H. Huang, M. I. Bodnarchuk, S. V. Kershaw, M. V. Kovalenko, A. L. Rogach, *ACS Energy Lett.* **2017**, *2*, 2071.

[6] G. R. Yettapu, D. Talukdar, S. Sarkar, A. Swarnkar, A. Nag, P. Ghosh, P. Mandal, *Nano Lett.* **2016**, *16*, 4838.

© 2024 The Author(s). Advanced Functional Materials published by Wiley-VCH GmbH

16163028, 0, Downloaded from https://onlinelibrary.wiley.com/doi/10.1002/adfm.202411319 by Universita Milano Bicocca, Wiley Online Library on [07/10/2024]. See the Terms and Conditions (https://onlinelibrary.wiley.com/terms-and-conditions) on Wiley Online Library for rules of use; OA articles are governed by the applicable Creative Commons License

[7] a) M. Baranowski, P. Plochocka, *Adv. Energy Mater.* **2020**, *10*, 1903659; b) B. P. Carwithen, T. R. Hopper, Z. Ge, N. Mondal, T. Wang, R. Mazlumian, X. Zheng, F. Krieg, F. Montanarella, G. Nedelcu, M. Kroll, M. A. Siguan, J. M. Frost, K. Leo, Y. Vaynzof, M. I. Bodnarchuk, M. V. Kovalenko, A. A. Bakulin, *ACS Nano* **2023**, *17*, 6638.

[8] a) F. Yan, S. T. Tan, X. Li, H. V. Demir, *Small* **2019**, *15*, 1902079; b) J. Pan, L. N. Quan, Y. Zhao, W. Peng, B. Murali, S. P. Sarmah, M. Yuan, L. Sinatra, N. M. Alyami, J. Liu, E. Yassitepe, Z. Yang, O. Voznyy, R. Comin, M. N. Hedhili, O. F. Mohammed, Z. H. Lu, D. H. Kim, E. H. Sargent, O. M. Bakr, *Adv. Mater.* **2016**, *28*, 8718; c) M. Cao, Y. Xu, P. Li, Q. Zhong, D. Yang, Q. Zhang, *J. Mater. Chem. C* **2019**, *7*, 14412; d) M. Liu, Q. Wan, H. Wang, F. Carulli, X. Sun, W. Zheng, L. Kong, Q. Zhang, C. Zhang, Q. Zhang, S. Brovelli, L. Li, *Nat. Photonics* **2021**, *15*, 379.

[9] a) M. Liu, G. Zhong, Y. Yin, J. Miao, K. Li, C. Wang, X. Xu, C. Shen, H. Meng, *Adv. Sci.* **2017**, *4*, 1700335; b) M. Lu, Y. Zhang, S. Wang, J. Guo, W. W. Yu, A. L. Rogach, *Adv. Funct. Mater.* **2019**, *29*, 1902008; c) Y. Gao, C. Huang, C. Hao, S. Sun, L. Zhang, C. Zhang, Z. Duan, K. Wang, Z. Jin, N. Zhang, A. V. Kildishev, C.-W. Qiu, Q. Song, S. Xiao, *ACS Nano* **2018**, *12*, 8847.

[10] a) N. Zhou, D. Wang, Y. Bao, R. Zhu, P. Yang, L. Song, *Adv. Opt. Mater.* **2023**, *11*, 2202681; b) F. Meinardi, Q. A. Akkerman, F. Bruni, S. Park, M. Mauri, Z. Dang, L. Manna, S. Brovelli, *ACS Energy Lett.* **2017**, *2*, 2368.

[11] a) C. Dujardin, E. Auffray, E. Bourret-Courchesne, P. Dorenbos, P. Lecoq, M. Nikl, A. N. Vasil'ev, A. Yoshikawa, R. Y. Zhu, *IEEE Trans. Nucl. Sci.* **2018**, *65*, 1977. b) M. Gandini, I. Villa, M. Beretta, C. Gotti, M. Imran, F. Carulli, E. Fantuzzi, M. Sassi, M. Zaffalon, C. Brofferio, L. Manna, L. Beverina, A. Vedda, M. Fasoli, L. Gironi, S. Brovelli, *Nat. Nanotechnol.* **2020**, *15*, 462; c) F. Cova, A. Erroi, M. L. Zaffalon, A. Cemmi, I. Di Sarcina, J. Perego, A. Monguzzi, A. Comotti, F. Rossi, F. Carulli, S. Brovelli, *Nano Lett.* **2024**, *24*, 905.

[12] a) M. Wu, N. Haji Ladi, Z. Yi, H. Li, Y. Shen, M. Wang, *Energy Technol.* **2020**, *8*, 1900744; b) X. Zhao, N.-G. Park, *Photonics* **2015**, *2*, 1139; c) B.-R. Jheng, P.-T. Chiu, S.-H. Yang, Y.-L. Tong, *Sci. Rep.* **2022**, *12*, 2921; d) T. A. Berhe, W.-N. Su, C.-H. Chen, C.-J. Pan, J.-H. Cheng, H.-M. Chen, M.-C. Tsai, L.-Y. Chen, A. A. Dubale, B.-J. Hwang, *Energy Environ. Sci.* **2016**, *9*, 323; e) H. Zhang, X. Wang, Q. Liao, Z. Xu, H. Li, L. Zheng, H. Fu, *Adv. Funct. Mater.* **2017**, *27*, 1604382.

[13] a) S. Liang, M. Zhang, G. M. Biesold, W. Choi, Y. He, Z. Li, D. Shen, Z. Lin, *Adv. Mater.* **2021**, *33*, 2005888; b) D. Yang, X. Li, H. Zeng, *Adv. Mater. Interfaces* **2018**, *5*, 1701662; c) Q. Zhou, Z. Bai, W.-g. Lu, Y. Wang, B. Zou, H. Zhong, *Adv. Mater.* **2016**, *28*, 9163.

[14] a) M. Rodová, J. Brožek, K. Knížek, K. Nitsch, *J. Therm. Anal. Calorim.* **2003**, *71*, 667; b) H. Zhao, D. Benetti, X. Tong, H. Zhang, Y. Zhou, G. Liu, D. Ma, S. Sun, Z. M. Wang, Y. Wang, F. Rosei, *Nano Energy* **2018**, *50*, 756.

[15] A. Erroi, S. Mecca, M. L. Zaffalon, I. Frank, F. Carulli, A. Cemmi, I. Di Sarcina, D. Debellis, F. Rossi, F. Cova, K. Pauwels, M. Mauri, J. Perego, V. Pinchetti, A. Comotti, F. Meinardi, A. Vedda, E. Auffray, L. Beverina, S. Brovelli, *ACS Energy Lett.* **2023**, *8*, 3883.

[16] a) F. Meinardi, A. Colombo, K. A. Velizhanin, R. Simonutti, M. Lorenzon, L. Beverina, R. Viswanatha, V. I. Klimov, S. Brovelli, *Nat. Photonics* **2014**, *8*, 392; b) F. Meinardi, H. McDaniel, F. Carulli, A. Colombo, K. A. Velizhanin, N. S. Makarov, R. Simonutti, V. I. Klimov, S. Brovelli, *Nat. Nanotechnol.* **2015**, *10*, 878; c) A. Colombo, F. Tassone, F. Santolini, N. Contiello, A. Gambirasio, R. Simonutti, *J. Mater. Chem. C* **2013**, *1*, 2927.

[17] a) K. Děcká, F. Pagano, I. Frank, N. Kratochwil, E. Mihóková, E. Auffray, V. Čuba, *J. Mater. Chem. C* **2022**, *10*, 12836; b) L. Zhao, Y.-W. Yeh, N. L. Tran, F. Wu, Z. Xiao, R. A. Kerner, Y. L. Lin, G. D. Scholes, N. Yao, B. P. Rand, *ACS Nano* **2017**, *11*, 3957; c) S. N. Raja, Y. Bekenstein, M. A. Koc, S. Fischer, D. Zhang, L. Lin, R. O. Ritchie, P. Yang, A. P. Alivisatos, *ACS Appl. Mater. Interfaces* **2016**, *8*, 35523.

[18] a) H. Liao, S. Guo, S. Cao, L. Wang, F. Gao, Z. Yang, J. Zheng, W. Yang, *Adv. Opt. Mater.* **2018**, *6*, 1800346; b) M. Meyns, M. Perálvarez, A. Heuer-Jungemann, W. Hertog, M. Ibáñez, R. Nafria, A. Genç, J. Arbiol, M. V. Kovalenko, J. Carreras, A. Cabot, A. G. Kanaras, *ACS Appl. Mater. Interfaces* **2016**, *8*, 19579.

[19] A. Anand, M. L. Zaffalon, A. Erroi, F. Cova, F. Carulli, S. Brovelli, *ACS Energy Lett.* **2024**, *9*, 1261.

[20] a) X. Peng, L. Hu, X. Sun, Y. Lu, D. Chu, P. Xiao, *ACS Appl. Nano Mater.* **2023**, *6*, 646; b) J. Wu, J. Tong, Y. Gao, A. Wang, T. Zhang, H. Tan, S. Nie, Z. Deng, *Angew. Chem., Int. Ed.* **2020**, *59*, 7738.

[21] a) H. Mokbel, F. Dumur, B. Raveau, F. Morlet-Savary, C. Simonnet-Jégat, D. Gigmes, J. Toufaily, T. Hamieh, J. P. Fouassier, J. Lalevée, *Tetrahedron* **2016**, *72*, 7686; b) Y.-C. Wong, J. De Andrew Ng, Z.-K. Tan, *Adv. Mater.* **2018**, *30*, 1800774.

[22] K. Parkatzidis, H. S. Wang, N. P. Truong, A. Anastasaki, *Chem* **2020**, *6*, 1575.

[23] a) A. Goto, T. Fukuda, *Prog. Polym. Sci.* **2004**, *29*, 329; b) A. M. Gregory, M. H. Stenzel, *Prog. Polym. Sci.* **2012**, *37*, 38; c) J. Nicolas, Y. Guillaneuf, C. Lefay, D. Bertin, D. Gigmes, B. Charleux, *Prog. Polym. Sci.* **2013**, *38*, 63; d) K. Matyjaszewski, *Macromolecules* **2012**, *45*, 4015; e) Y. Deng, S. Schäfer, D. Kronstein, A. Atabay, M. Susewind, E. Krieg, S. Seiffert, J. Gaitzsch, *Biomacromolecules* **2024**, *25*, 303.

[24] a) V. Bellotti, R. Simonutti, *Polymers* **2021**, *13*, 1119; b) N. P. Truong, G. R. Jones, K. G. E. Bradford, D. Konkolewicz, A. Anastasaki, *Nat. Rev. Chem.* **2021**, *5*, 859; c) K. Sparnacci, T. Frison, E. Podda, D. Antonioli, M. Laus, M. Notari, G. Assanelli, M. Atzeni, G. Merlini, R. Pó, *ACS Appl. Polym. Mater.* **2022**, *4*, 8722.

[25] Y. Zhu, Y. Liu, K. A. Miller, H. Zhu, E. Egap, *ACS Macro Lett.* **2020**, *9*, 725.

[26] a) X. Jin, K. Ma, J. Chakkamalayath, J. Morsby, H. Gao, *ACS Energy Lett.* **2022**, *7*, 610; b) X. Jin, K. Ma, H. Gao, *J. Am. Chem. Soc.* **2022**, *144*, 20411.

[27] a) V. Bellotti, G. Beretta, R. Simonutti, *Polymer* **2023**, *271*, 125804; b) J. Xu, K. Jung, A. Atme, S. Shanmugam, C. Boyer, *J. Am. Chem. Soc.* **2014**, *136*, 5508; c) K. Parkatzidis, N. P. Truong, M. N. Antonopoulou, R. Whitfield, D. Konkolewicz, A. Anastasaki, *Polym. Chem.* **2020**, *11*, 4968.

[28] V. Bellotti, C. Daldossi, D. Perilli, M. D'Arienzo, M. Stredansky, C. Di Valentin, R. Simonutti, *J. Catal.* **2023**, *428*, 115074.

[29] M. P. U. Haris, E. Ruiz, S. Kazim, S. Ahmad, *Cell Rep. Phys. Sci.* **2023**, *4*, 101516.

[30] S. Mecca, F. Pallini, V. Pinchetti, A. Erroi, A. Fappani, F. Rossi, S. Mattiello, G. M. Vanacore, S. Brovelli, L. Beverina, *ACS Appl. Nano Mater.* **2023**, *6*, 9436.

[31] a) F. Ye, H. Zhang, W. Li, Y. Yan, J. Cai, R. S. Gurney, A. J. Pearson, D. Liu, T. Wang, *Small Methods* **2019**, *3*, 1800489; b) F. Di Stasio, S. Christodoulou, N. Huo, G. Konstantatos, *Chem. Mater.* **2017**, *29*, 7663; c) F. Fang, W. Chen, Y. Li, H. Liu, M. Mei, R. Zhang, J. Hao, M. Mikita, W. Cao, R. Pan, K. Wang, X. W. Sun, *Adv. Funct. Mater.* **2018**, *28*, 1706000.

[32] W. Y. Chiu, G. M. Carratt, D. S. Soong, *Macromolecules* **1983**, *16*, 348.

[33] M. Hartlieb, *Macromol. Rapid Commun.* **2022**, *43*, 2100514.

[34] L. Lu, M. Sun, T. Wu, Q. Lu, B. Chen, B. Huang, *Nanoscale Adv.* **2022**, *4*, 680.

[35] M. Nikl, A. Yoshikawa, *Adv. Opt. Mater.* **2015**, *3*, 463.

[36] a) T. J. Hajagos, C. Liu, N. J. Cherepy, Q. Pei, *Adv. Mater.* **2018**, *30*, 1706956; b) N. P. Zaitseva, A. M. Glenn, A. N. Mabe, M. L. Carman, C. R. Hurlbut, J. W. Inman, S. A. Payne, *Nucl. Instrum. Methods Phys. Res., Sect. A* **2018**, *889*, 97.

[37] G. F. Knoll, *Radiation Detection and Measurement*, John Wiley and Sons, New York, USA **2010**.

© 2024 The Author(s). Advanced Functional Materials published by Wiley-VCH GmbH

16163028, 0, Downloaded from https://onlinelibrary.wiley.com/doi/10.1002/adfm.202411319 by Universita Milano Bicocca, Wiley Online Library on [07/10/2024]. See the Terms and Conditions (https://onlinelibrary.wiley.com/terms-and-conditions) on Wiley Online Library for rules of use; OA articles are governed by the applicable Creative Commons License

[38] a) S. Alawabdeh, *Characterization and Comparison of Proton Light Yield of Similar Composition Organic Scintillators with Different Sizes*, North Carolina State University, Raleigh, USA **2023**; b) J. A. Brown, T. A. Laplace, B. L. Goldblum, J. J. Manfredi, T. S. Johnson, F. Moretti, A. Venkatraman, *Nucl. Instrum. Methods Phys. Res., Sect. A* **2023**, *1054*, 168397.

[39] a) M. L. Zaffalon, F. Cova, M. Liu, A. Cemmi, I. Di Sarcina, F. Rossi, F. Carulli, A. Erroi, C. Rodà, J. Perego, A. Comotti, M. Fasoli, F. Meinardi, L. Li, A. Vedda, S. Brovelli, *Nat. Photonics* **2022**, *16*, 860; b) C. Rodà, M. Fasoli, M. L. Zaffalon, F. Cova, V. Pinchetti, J. Shamsi, A. L. Abdelhady, M. Imran, F. Meinardi, L. Manna, A. Vedda, S. Brovelli, *Adv. Funct. Mater.* **2021**, *31*, 2104879.

[40] A. Erroi, F. Carulli, F. Cova, I. Frank, M. L. Zaffalon, J. Llusar, S. Mecca, A. Cemmi, I. Di Sarcina, F. Rossi, L. Beverina, F. Meinardi, I. Infante, E. Auffray, S. Brovelli, *ACS Energy Lett.* **2024**, *9*, 2333.

[41] E. Auffray, B. Frisch, F. Geraci, A. Ghezzi, S. Gundacker, H. Hillemanns, P. Jarron, T. Meyer, M. Paganoni, K. Pauwels, M. Pizzichemi, P. Lecoq, *IEEE Trans. Nucl. Sci.* **2013**, *60*, 3163.

[42] P. Lecoq, C. Morel, J. O. Prior, D. Visvikis, S. Gundacker, E. Auffray, P. Križan, R. M. Turtos, D. Thers, E. Charbon, J. Varela, C. de La Taille, A. Rivetti, D. Breton, J.-F. Pratte, J. Nuyts, S. Surti, S. Vandenberghe, P. Marsden, K. Parodi, J. M. Benlloch, M. Benoit, *Phys. Med. Biol.* **2020**, *65*, 21RM01.

© 2024 The Author(s). Advanced Functional Materials published by Wiley-VCH GmbH

16163028, 0, Downloaded from https://onlinelibrary.wiley.com/doi/10.1002/adfm.202411319 by Universita Milano Bicocca, Wiley Online Library on [07/10/2024]. See the Terms and Conditions (https://onlinelibrary.wiley.com/terms-and-conditions) on Wiley Online Library for rules of use; OA articles are governed by the applicable Creative Commons License